In-Situ Nuclear Magnetic Resonance Investigation of Strain, Temperature, and Strain-Rate Variations of Deformation-Induced Vacancy Concentration in Aluminum

K. LINGA MURTY, K. DETEMPLE, O. KANERT, and J.Th.M. DEHOSSON

Critical strain to serrated flow in solid solution alloys exhibiting dynamic strain aging (DSA) or Portevin–LeChatelier effect is due to the strain-induced vacancy production. Nuclear magnetic resonance (NMR) techniques can be used to monitor *in situ* the dynamical behavior of point and line defects in materials during deformation, and these techniques are nondestructive and noninvasive. The new CUT-sequence pulse method allowed an accurate evaluation of the strain-enhanced vacancy diffusion and, thus, the excess vacancy concentration during deformation as a function of strain, strain rate, and temperature. Due to skin effect problems in metals at high frequencies, thin foils of Al were used and experimental results correlated with models based on vacancy production through mechanical work (*vs* thermal jogs), while *in situ* annealing of excess vacancies is noted at high temperatures. These correlations made it feasible to obtain explicit dependencies of the strain-induced vacancy concentration on test variables such as the strain, strain rate, and temperature. These studies clearly reveal the power and utility of these NMR techniques in the determination of deformation-induced vacancies *in situ* in a noninvasive fashion.

I. INTRODUCTION

IN an earlier article, we reported the results on enhanced diffusion during deformation of bulk single crystalline alkali halides (NaCl and NaF) and demonstrated the applicability of nuclear magnetic resonance (NMR) pulse techniques in evaluating the concentration of deformation-induced excess vacancies.[1] In addition, preliminary results obtained on thin foils of Al were briefly pointed out. Now, we report here the strain, strain-rate, and temperature variations of the excess vacancy concentration derived from NMR pulse experiments using the new CUT-sequence method. These results on the strain-induced vacancy concentration have important bearing on the understanding of the dynamic strain aging (DSA) and the development of quantitative models characterizing the DSA.[2,3] In particular, the critical strain (ε_c) for the onset of serrations is related to the strain-induced vacancy concentration and mobile dislocation density:[2,3]

$$\dot{\varepsilon} = A\varepsilon_c^{m+\beta} \exp\left(-\frac{E_m}{kT}\right),\ C_V^{\varepsilon} \propto \varepsilon_c^{m},\ \text{and}\ \rho_m \propto \varepsilon_c^{\beta} \quad [1]$$

Here, C_v^{ε} is the strain-induced vacancy concentration, ρ_m is the density of mobile dislocations, and E_m is the activation energy for vacancy migration. The constants $m + \beta$ and E_m are generally evaluated from the strain-rate and temperature dependencies of the critical strain on serrated flow in tensile tests. The present study enables an evaluation of the strain-induced vacancy concentration rather directly. Moreover, the excess vacancies resulting in enhanced diffusion have strong influence on the creep behavior of metals and ceramics in that the activation energy for creep decreases with increased stress or strain rate if the concentration of these nonequilibrium vacancies is significant.[4–7]

The dynamical behavior of point defects in metals is usually characterized by investigating annealing kinetics following extensive cold work. The recovery of induced plastic deformation is monitored using various techniques such as electrical resistivity,[8] positron lifetimes,[9] perturbed-angular correlation,[10] Mossbauer spectroscopy,[11] ultrasonic attenuation,[12] *etc.* In contrast to these *two-step experiments*, it is desirable to be able to investigate these kinetics *in situ* during deformation of materials in a single step. The plethora of nondestructive experimental techniques notwithstanding, very few of them are useful in the investigation of the *dynamical* properties of these defects. This is particularly true in the investigation of the diffusion of point defects and motion of dislocations.

Nuclear spin resonance methods have been used extensively to investigate the diffusion of point defects in solids at high temperatures, localized motion of atomic defects at low temperatures, and motion of line defects (dislocations) during deformation.[13] Nuclear magnetic resonance has been recognized as one of the most powerful techniques for diffusion studies in materials and has been extensively used to determine various diffusion parameters such as the activation energies for diffusion in both nonmetals and metals.[14,15] Murty and Ruoff[16] applied the NMR pulse techniques to determine the activation volumes for motion and formation of Schottky defect pairs by evaluating the effects of test temperature superimposed by hydrostatic pressure. Since NMR probes the rate of atomic jumps rather directly, one can in principle obtain a better microscopic picture of the diffusional process. Later advances leading to the evaluation of the spin-lattice relaxation times in ro-

K. LINGA MURTY is Professor, Department of Nuclear Engineering and Department of Materials Science & Engr., with North Carolina State University, Raleigh, NC 27695-7909. K. DETEMPLE, Graduate Research Assistant, and O. KANERT, Professor, are with the Department of Physics, University of Dortmund, 44221 Dortmund, Federal Republic of Germany. J.Th.M. DEHOSSON, Professor, is with the Department of Applied Physics, University of Groningen, 9747 AG Groningen, The Netherlands

Manuscript submitted May 8, 1997

tating frame resulted in high sensitivity of this parameter to atomic jump processes. Rowland and Fradin,[17] Kanert,[13] and others were thus able to evaluate the impurity diffusion in alloys. These techniques, in addition, made it possible to investigate the dislocation jump distances *in situ* during deformation in a noninvasive fashion.[18,19,20] We have recently reported an investigation of the superimposed effects of deformation on spin-lattice relaxation times in the rotating frame ($T_1\rho$) in single crystalline pure ($\approx$1.5 ppm impurity) NaCl and NaF at varied temperatures and strain rates,[1] from which the strain-induced excess vacancy concentration was derived. In this study, both the classic $T_1\rho$ and the new CUT-sequence methods were used, while the data analyses were based on the vacancy production due to both the thermal and mechanical jogs.[3] Analyses of the mechanical-jog based vacancy production were shown to be in agreement with the experimental results in NaCl and NaF.[1]

In this article, we describe the strain, strain-rate, and test temperature variations of strain-induced vacancy concentration in aluminum derived from the nuclear spin relaxation (NSR) rates determined using the CUT-sequence technique. As pointed out earlier,[1,21] skin effect problems preclude usage of bulk metallic samples, and thus, thin foils of aluminum need to be used, which makes it relatively more difficult to perform NMR-deformation experiments. While the majority of the data analyses is based on the Estrin–Mecking model[3] of vacancy generation due to mechanically produced jogs, predictions based on vacancy production due to thermal jogs are also briefly outlined. The choice of Al is based on the fact that it is a suitable nucleus for magnetic resonance studies. In addition, the thermal vacancy concentration is well established in Al, and the dynamic strain aging studies of aluminum alloys have been prevalent.[22] Moreover, the effect of stress on the activation energy for creep has been widely studied to derive the strain and strain-rate effects on nonequilibrium vacancy concentration.[23]

II. SPIN RELAXATION RATE AND ATOMIC DIFFUSION

The nuclear spin relaxation rate in the rotating frame ($1/T_1\rho$) is related to the atomic jump rate, Γ,[13] and in the Torrey approach, for $\Gamma < \omega_{\text{eff}}$, we find[21]

$$\frac{1}{T_{1\rho}^{\text{diff}}} = A(\omega_1)\,\frac{<\omega_\rho^2>}{4\,\omega_{\text{eff}}^2}\,\Gamma \qquad [2]$$

Here, $\langle\omega_\rho^2\rangle$ denotes the-mean-square spin interaction responsible for the relaxation process; $\omega_{\text{eff}} \propto \sqrt{\omega_1^2 + \omega_{\text{loc}}^2}$ is the effective Larmor frequency in the rotating frame, with $\omega_1 = \gamma B_1$ being the external frequency due to locking field B_1, γ being the gyromagnetic ratio of the spins.

The atomic jump rate in metals is proportional to the concentration (C_v) of monovacancies:

$$\Gamma = C_v\,\Gamma_v \qquad [3]$$

where Γ_v is the jump rate of vacancies. The vacancy jump rate follows the Arrhenius relation

$$\Gamma_v = \Gamma_0 \exp\left(-\frac{E_m}{kT}\right) \qquad [4]$$

where E_m is the activation energy for vacancy migration and Γ_0 is the attempt frequency of the process. Vacancies exist in thermal equilibrium, and thus,

$$C_v^0 = \exp\left(-\frac{E_f}{kT}\right) \qquad [5]$$

Here, E_f is the vacancy formation energy. Thus, the higher the temperature, the larger is the vacancy concentration and the faster is the atomic jump rate, leading to rapid atomic transport.

The superscript, o, in Eq. [5] indicates thermal equilibrium, and additional vacancies can be formed by various processes such as quenching, irradiation, plastic deformation, *etc.* We are concerned here with the excess nonequilibrium vacancies due to deformation (C_v^ε), and these additional vacancies resulted in increased rates of atomic jumps (Eq. [3]). Assuming that the jump rate of vacancies remains unaltered, the atomic jump frequency in Eq. [3] can be rewritten as

$$\Gamma = (C_v^0 + C_v^\varepsilon)\,\Gamma_v = C_v^{\text{total}}\,\Gamma_v \qquad [6]$$

Thus, the NSR due to diffusion in Eq. [2] has two terms:

$$\frac{1}{T_{1\rho}^{\text{diff}}} = \frac{1}{T_{1\rho}^{\text{diff}}}\Big)_0 + \frac{1}{T_{1\rho}^{\text{diff}}}\Big)_\varepsilon \qquad [7a]$$

and, thus, according to Eq. [2]

$$\begin{aligned}\frac{1}{T_{1\rho}^{\text{diff}}} &= A\,(\omega_1)\,\frac{<\omega_\rho^2>}{4\,\omega_{\text{eff}}^2}\,\Gamma_v\,C_v^{\text{total}} \\ &= A'\,\Gamma_v\,(C_v^0 + C_v^\varepsilon)\end{aligned} \qquad [7b]$$

The strain-induced excess vacancy concentration, thus, can be evaluated from the experimental evaluation of the relaxation rate ($1/T_{1\rho}^{\text{diff}}$) with and without deformation and by subtracting the thermal contribution (*i.e.*, without deformation). However, additional processes may contribute to the total relaxation rates, and these need to be taken into account. In metals, the conduction-electron contribution dominates at low temperatures and follows the Korringa relation

$$\frac{1}{T_{1\rho}^{ce}} = A(\omega_1)\,CT \qquad [8]$$

where C is a material constant. Thus, one measures the relaxation rates before and during deformation and finds the deformation-induced relaxation rate by subtracting the background relaxation, which consists of thermal equilibrium diffusion and other processes.

III. STRAIN-INDUCED VACANCIES

Plastic deformation results in an increased number of vacancies that are produced from climbing jogs on dislocations.[2–6,24] While theoretical analyses[23] clearly point to the strain-enhanced diffusion due to the excess vacancies produced during plastic deformation, experimental studies (tracer diffusion, creep, *etc.*) failed to yield consistent results,[25,26,27] and Ruoff[4] and Ruoff and Balluffi[23] cited experimental data on creep, which exhibited no such presence of excess vacancies.[6] The present and earlier NMR studies,[21,24] however, clearly revealed the increased vacancy concentration during deformation and made it possible to

establish a quantitative relation between the strain-induced vacancy concentration and the applied strain rate, strain, and temperature.

The excess athermal vacancies produced during deformation migrate to sinks such as the jogs on dislocations. Thus, the strain-induced vacancy concentration follows the rate equation

$$\dot{C}_v^{\varepsilon} = \dot{C}_v^{\varepsilon}\Big|^{+} + \dot{C}_v^{\varepsilon}\Big|^{-} \qquad [9]$$

where the superscript + and − indicate the production and annihilation, respectively. The formation process is governed by the nonconservative motion of jogs on screw dislocations, and the rate of production is proportional to the applied strain rate:[2]

$$\dot{C}_v^{\varepsilon}\Big|^{+} = \alpha(T, \varepsilon)\,\dot{\varepsilon} \qquad [10]$$

where α is a strain- (and also perhaps temperature-) dependent parameter proportional to the concentration of jogs.

Different approaches have been considered in the literature concerning the coefficient α depending on the mechanism of jog production.[21] Mecking and Estrin[3] assume that the jogs are produced mechanically by the applied work so that α will be temperature independent and proportional to the applied stress and inversely to the jog energy:

$$\dot{C}_v^{\varepsilon}\Big|^{+}_{\text{mech}} = \alpha_1 \frac{\sigma}{E_j}\,\dot{\varepsilon},\; E_j = 0.1\,G\mathbf{b}^3 \qquad [11]$$

where G is the shear modulus; $\mathbf{b}$ is the Burgers vector; α_1 is a constant of the order of 0.1, describing the fraction of the mechanical work used for jog formation; and E_J is the jog formation energy. With $\sigma \propto \sqrt{\rho}$, we find

$$\dot{C}_v^{\varepsilon}\Big|^{+}_{\text{mech}} = \alpha_1 \frac{\sqrt{\rho}}{E_j}\,\dot{\varepsilon},\; \rho = \rho(\varepsilon) \qquad [12]$$

where ρ is the dislocation density, which depends on plastic strain. Other variations of this equation were suggested by Lenasson[28] and Murty *et al.*[2] If, on the other hand, we consider thermally produced jogs,[24] we find

$$\dot{C}_v^{\varepsilon}\Big|^{+}_{th} = \alpha_2\,\dot{\varepsilon}\,\exp\left(-\frac{E_j}{\mathrm{k}T}\right) \qquad [13]$$

While the various models differ with regard to the vacancy production, there is common agreement that these excess athermal vacancies disappear *via* diffusion to appropriate sinks. Thus, the concentration of these excess vacancies decreases with increased temperatures. While grain boundaries could act as vacancy sinks, in general, dislocations are the primary sinks for the annihilation of the vacancies:[2]

$$\dot{C}_v^{\varepsilon}\Big|^{-} = -\beta_0 \frac{\Gamma_v}{\lambda^2} C_v^{\varepsilon} \qquad [14]$$

where Γ_v is the vacancy jump frequency given by $\Gamma_v = \Gamma_{v0} \exp(-E_m/\mathrm{k}T)$, E_m being migration energy; β_0 is a coefficient independent of the test conditions; and λ is the sink distance given by the strain-dependent dislocation density ($\lambda^2 \approx \frac{1}{\rho}$). The strain dependence of the dislocation density is given by[29]

$$\frac{d\rho}{d\varepsilon} = a\sqrt{\rho} - c\,(\dot{\varepsilon}, T)\,\rho \qquad [15]$$

which implies that the dislocations are produced by the applied stress ($\propto\sqrt{\rho}$), while they anneal through first-order kinetics. The solution to Eq. [15] is found to be

$$\rho(\varepsilon) = \rho_{eq}\left\{1 - \frac{\sqrt{\rho_{eq}} - \sqrt{\rho_0}}{\sqrt{\rho_{eq}}}\exp\left(-\frac{c\varepsilon}{2}\right)\right\}^2 \qquad [16]$$

where $\rho_{eq} = a^2/c^2$ and ρ_0 is the initial dislocation density ($\varepsilon = 0$). The annihilation coefficient, c, is dependent on temperature and strain rate. The dislocation density increases linearly with strain until it reaches a saturation value.

In the previous analyses,[1] we assumed a steady-state condition, $C_v^{\dot{\varepsilon}} = 0$. However, recent studies revealed that one has to consider a nonsteady-state condition ($C_v^{\dot{\varepsilon}} \neq 0$) in order to interpret the data correctly. Solutions to the model equations were found for $\rho_{eq} >> \rho_0$ for both the mechanical jog formation and thermal jog production cases for low (2 pct) and high (20 pct) strains. These results are plotted in Figures 1(a) and (b), respectively, for the mechanical and thermal jog models.

We note that both models differentiate the behaviors at low *vs* high temperature regions. In both models, above a transition temperature, T^*, $C_v^{\dot{\varepsilon}}$ is thermally activated and increases linearly with strain rate and inverse temperature. At lower temperatures, the mechanical jog model predicts strain-rate- and temperature-independent excess vacancy concentration, which increases with strain. An Arrhenius type of relation is found for the thermal jog model; again, the higher the strain, the larger is the strain-induced vacancy concentration.

At high temperatures, the following expressions are found for C_v^{ε}. For the mechanical jog model,

$$C_v^{\varepsilon}\Big\}_{\text{high } T} = \frac{\alpha_1}{\beta_0\sqrt{\rho_{eq}}}\left\{1 - \exp\left(-\frac{b}{2}\varepsilon\right)\right\}\exp\left(\frac{E_m}{\mathrm{k}T}\right) \qquad [17a]$$

and for the thermal jog model,

$$C_v^{\varepsilon}\Big\}_{\text{high } T} = \frac{\alpha_2}{\beta_0} \qquad [17b]$$

In the low-temperature regime, we find the following expressions. For the mechanical jog model,

$$C_v^{\varepsilon}\Big\}_{\text{low } T} = \frac{\alpha_1}{\beta_0}\sqrt{\rho_{eq}}\;\;\varepsilon \qquad [18a]$$

and for the thermal jog model,

$$C_v^{\varepsilon}\Big\}_{\text{low } T} = \frac{\alpha_2}{\beta_0} \qquad [18b]$$

We note from Figure 1 that in both cases, the transition temperature, T^*, is a function of both the strain and strain rate.

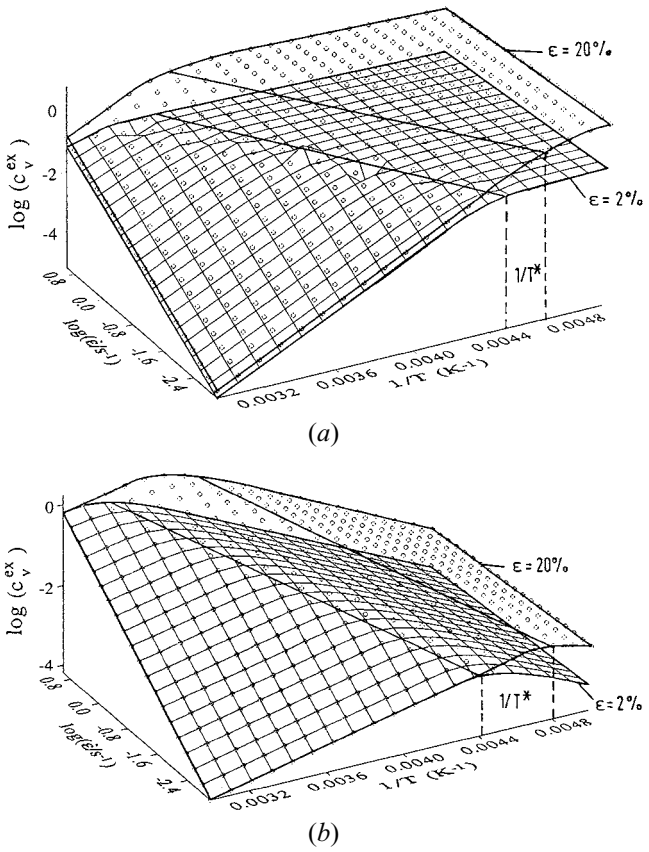

(*a*)

(*b*)

Fig. 1—(*a*) Strain-induced vacancy concentration as a function of strain rate and inverse temperature (mechanical jog model). (*b*) Strain-induced vacancy concentration as a function of strain rate and inverse temperature (thermal jog model).

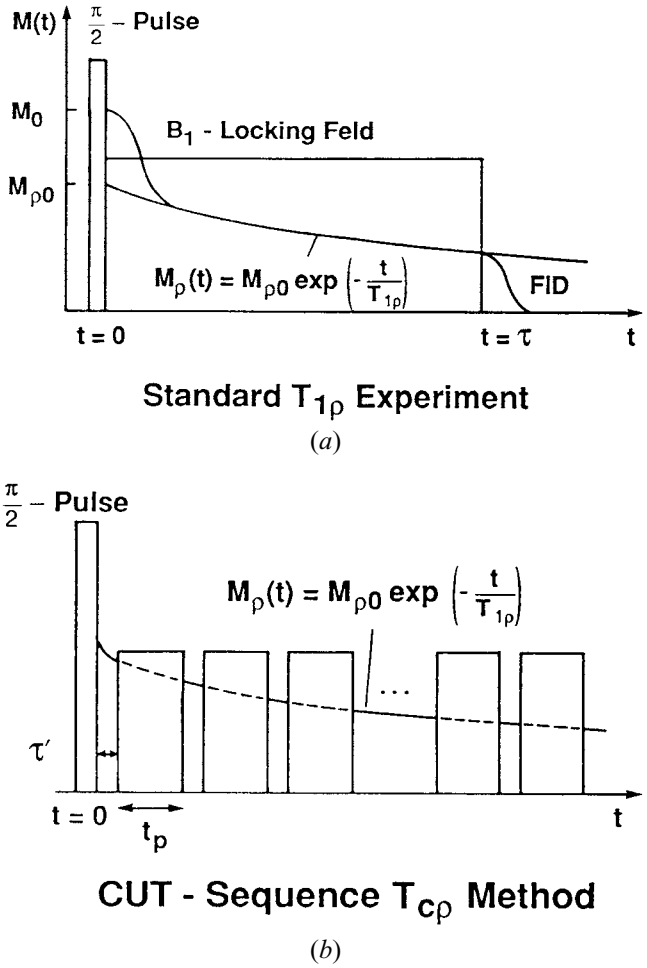

(*a*)

(*b*)

Fig. 2—(*a*) Sequence of pulses used in the traditional $T_{1\rho}$ method. (*b*) Pulses used in the current CUT-sequence method ($T_{c\rho}$).

IV. EXPERIMENTAL DETAILS

Ultrapure (99.999 pct) polycrystalline 25-mm-thick aluminum foil with a grain size of the order of 100 μm is used to avoid skin-effect problems associated with the NMR signal at these frequencies. Rectangular samples measuring 27 × 12 mm are deformed at a constant strain rate by a servohydraulic tensile machine developed for NMR experiments at varied temperatures (low and high).[18] Before and after each experiment, the background contribution was measured at the test temperature by setting $\dot{\varepsilon} = 0$.

A new CUT-sequence method was developed for accurate determination of NSR by modifying the spin-locking technique usually adopted for relaxation time measurements in the rotating frame. The traditional $T_{1\rho}$ method consists of a short $\pi/2$ pulse, which rotates the magnetization by 90 deg (*i.e.*, into the *y* direction of the rotating frame perpendicular to the applied magnetic field B_0). The pulse is followed by an rf (radio-frequency) field of strength B_1 (locking pulse) for a period *t* (Figure 2(a)) shifted in phase by 90 deg with respect to the $\pi/2$ pulse (*i.e.*, the locking field is aligned with the nuclear magnetization). The magnetization relaxes in the *locked* state with relaxation time $T_{1\rho}$, as follows:

$$M_\rho(t) = M_\rho(\mathrm{o}) \exp\left(-\frac{t}{T_{1\rho}}\right) \qquad [19]$$

where *M* is the nuclear magnetization. In Eq. [19], $M_{\rho 0}$ is the initial magnetization at the beginning ($t = 0$) of the locking field, which is often taken to be the signal height (M_0) following the $\pi/2$ pulse, whereas in reality it may be quite different from M_0. Moreover, in order to measure $M_\rho(t)$ at different times, one has to repeat the experiment varying the period τ of the locking pulse (Figure 2).

These problems are eliminated in the new CUT-sequence method, where the locking field is cut into a large number of short pulses with a known separation or *observation window* (Figure 2(b)). The time window t_w is far shorter than the pulse duration, t_p, such that

$$t_w << T_2, t_p \qquad [20]$$

where T_2 is the spin-spin relaxation time. The relaxation times thus measured agree exactly with those determined using the traditional method. A single-shot experiment thus provides *n* (the number of pulses) values of the decay function of $M_\rho(t)$. Such types of pulse sequences were used in the past for completely different types of tests.[30,31,32] More details on the method may be found in Reference 21.

Figure 3 depicts the time evolution of $M_\rho(t)$ of Al in aluminum measured with the single-shot CUT-sequence method at two temperatures at 41 MHz frequency with $B_0 = 3.7$ *T* (no deformation). Other parameters of the pulse sequence are $t_\rho = 20$ μs, $t_w = 8$ μs, and $B_1 = 4.5$ G. As is clear from Figure 2, the single-shot method makes it feasible to obtain the entire time evolution of the magnet-

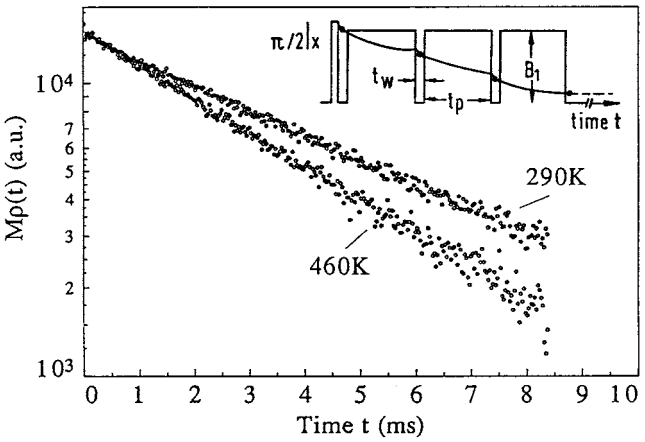

Fig. 3—Nuclear magnetization decay of Al using the single-shot CUT-sequence method at 290 and 460 K (no deformation).

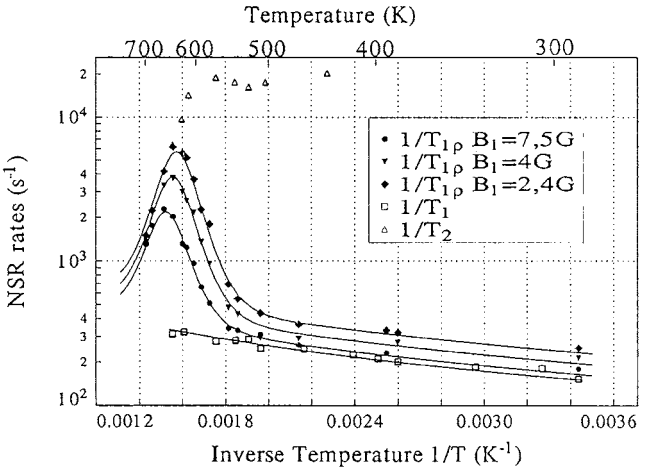

Fig. 4—Temperature variation of T_2, T_1, and $T_{1\rho}$.

ization M_ρ and thus eliminates uncertainties about the initial magnetization, M_0, and the exponential decay of the magnetization.

V. RESULTS AND DISCUSSION

A. *Temperature Variation of NSR ($\varepsilon = 0$)*

The NSRs were first measured without deformation as a function of test temperature. Spin-spin (T_2), spin-lattice (T_1), and spin-lattice relaxation times in rotating frame using the CUT-sequence method ($T_{1\rho}$) were determined. Figure 4 depicts the temperature dependence of these relaxation rates. Below about 550 K, the spin-lattice relaxation rates are caused by conduction electrons (Korringa relaxation process: $1/T_1 \propto T$), while $1/T_2$ is given by the *rigid* line width. However, at higher temperatures, $1/T_2$ decreased due to the motional narrowing of the line width, and $1/T_{1\rho}$ exhibited a dramatic increase with the characteristic peak (diffusion-induced relaxation processes[1,2]). The time T_1 failed to demonstrate this relaxation contribution and is controlled by a conduction-electron mechanism in the entire temperature regime. The effect of locking field (B_1) is clearly delineated in the $T_{1\rho}$ data.

The solid lines in Figure 4 are best-fit lines with NMR derived constants,[21] and the atomic jump rate is given by

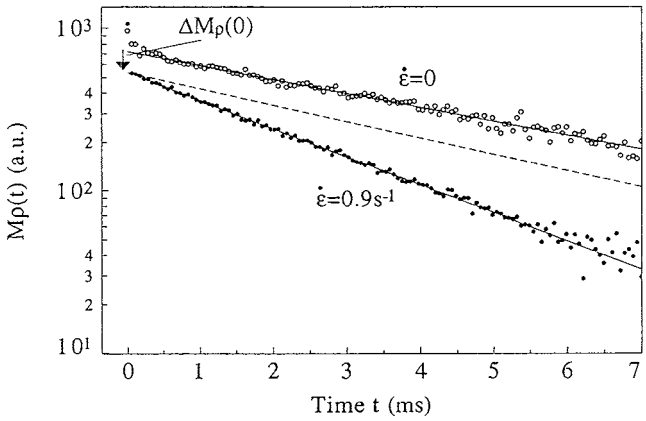

Fig. 5—Nuclear magnetization decay before and during deformation at 300 K.

$$\Gamma = \Gamma_0 \exp\left(\frac{S_f}{kT}\right) \exp\left(-\frac{E_m + E_f}{kT}\right) \qquad [21]$$

or

$$\Gamma = 4.65 \times 10^{14} \exp\left(-\frac{1.27\ \text{eV}}{kT}\right) \qquad [21a]$$

The activation energy for diffusion, 1.27 eV, is in excellent agreement with that obtained earlier using the traditional $T_{1\rho}$ method, as well as those reported by Fradin and Rowland.[33] This value is also identical to that for diffusion in aluminum determined by other techniques including high-temperature creep.[34]

B. *NMR-Deformation Experiments*

The NSR measurements were made at various temperatures and strain rates, and mechanical deformation led to increased rates of decay of magnetization or relaxation. An example is shown in Figure 5 for Al before and during deformation (0.9 s^{-1}) at 300 K. We note here two distinct features of the magnetic induction decay during deformation. Deformation created an offset $\Delta M_\rho(0)$ of the magnetization. Second, the increase in strain with time led to a slight increase in the slope of the background magnetization decay. The contribution of the strain-enhanced diffusion to the relaxation rate is then obtained by subtracting the total background decay (dashed line in Figure 5) from the slopes of the decay measured during deformation.

Thus, the diffusion-induced excess relaxation time, $T_{1\rho}^{(\text{diff})}{}_\varepsilon$, of Al is measured during deformation as a function of the test temperature, strain rate, and strain. Temperature variation of this excess relaxation rate is shown in Figure 6 for a constant strain rate of 0.55 s^{-1} at two strains, 0.6 and 3 pct. It is clear that the relaxation rate increases with strain and falls rapidly at high temperatures, implying that the strain-induced vacancy concentration increases with strain while it decreases rapidly as temperature increases. The decrease at high temperatures is due to the annihilation of these excess vacancies because of the increased migration rates. The composite effects of the strain rate and strain of the excess relaxation rate are illustrated in Figure 7 for 290 and 385 K. The contour net in this figure represents a best fit to the data using the model based on mechanical jog formation.

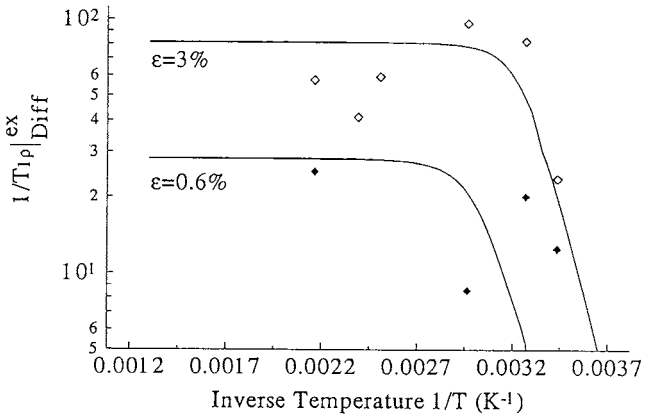

Fig. 6—Temperature variation of excess NSR rate due to deformation in Al at 0.55 s^{-1} for 0.6 and 3 pct strains.

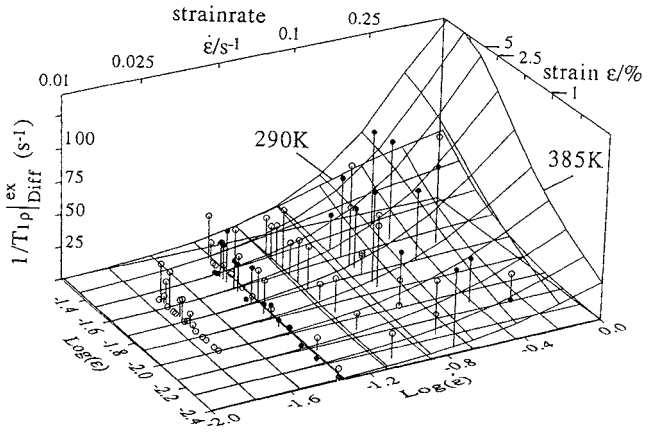

Fig. 7—NSR rate due to deformation in Al as a function of strain rate and strain at 290 and 385 K (contours are fit to the model).

Table I. Parameters Derived from NSR Data

Parameter	Value
ρ_{eq}	3.4×10^{16} m^{-2}
β_0	8.3×10^{-20} m^2
α_1	0.33 $G\mathbf{b}$
G	2.8×10^4 MPa
$\mathbf{b}$	0.286 nm
α/E_j	5.4×10^{-8}

C. *Strain-Induced Vacancy Concentration in Al*

Correlations of the experimental results with the model predictions based on mechanical and thermal jogs revealed good agreement with the mechanical jog model. The experimental results, as shown in Figures 6 and 7, are fit to the model from which the complete solution to the strain-induced vacancy concentration is obtained:

$$C_v^{\varepsilon} = C_{veq}^{\varepsilon} \left\{1 - (1 - c_2) \exp(-\beta_0 \rho_{eq} \Gamma_v^{\varepsilon}) - c_2 \exp\left(-\frac{c}{2}\varepsilon\right)\right\} \quad [22]$$

where

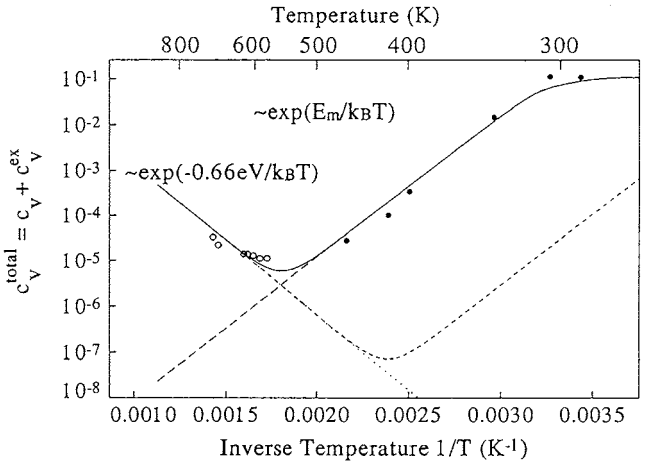

Fig. 8—Arrhenius plot of total vacancy concentration: experimental results compared with predictions based on the mechanical jog (Estrin–Mecking) model (solid line at 0.55 s^{-1} and dashed line at 10^{-4} s^{-1})

$$C_{veq}^{\varepsilon} = \frac{\alpha_1}{E_j \sqrt{\rho_{eq}}\, \Gamma_v} \quad [22a]$$

$$c_1 = \frac{1}{1 - (c/2\ \beta_0\ \rho_{eq}\ \Gamma_v)\,\dot{\varepsilon}} \quad [22b]$$

and

$$\Gamma_v = 2 \times 10^{14} \exp\left(-\frac{0.62\ \text{eV}}{kT}\right),\ s^{-1} \quad [22c]$$

The solid lines in Figures 6 and 7 are obtained from the best fit to the data of Eq. [22]. The parameters obtained from these data analyses are summarized in Table I. The high- and low-temperature approximations are evaluated using the various constants in the table in Eq. [22]. We find for the vacancy concentration in the high-temperature region,

$$C_V^{\varepsilon}\Big\}_{\text{high } T} = \frac{3.6 \times 10^3}{\Gamma_v}\,[1 - c_2 \exp(-43\ \varepsilon)] \quad [23a]$$

This is in agreement with the mechanical jog model prediction, as noted in Eq. [17a]. It should be pointed out that the NSR rate due to deformation does not depend on the temperature, since Γv cancels out (Eqs. [7b] and [2a]).

In the low-temperature regime, where $0.003\ \Gamma_v \varepsilon << \dot{\varepsilon}$, we find

$$C_V^{\varepsilon}\Big\}_{\text{low } T} = 9.7\ \varepsilon \quad [23b]$$

in agreement with Eq. [17b], as derived from the model based on mechanical jog formation.

The analysis of the data yields a value of 1.3×10^{-27} m^3 for α_1 in the model equation (Eq. [12]), recollecting the fact that this factor represents the efficiency of the mechanical work in jog formation and vacancy creation. With a value of 1.6×10^{-25} m^3 for typical volume ($\approx \rho_{eq}^{-3/2}$), we find that the efficiency is about 1 pct.

Finally, in order to illustrate the temperature regimes where thermal vacancies and strain-induced vacancies dominate, we depict the temperature variation of the total vacancy concentration (C_v^{total}) in Figure 8 as an Arrhenius plot.

Here, we used the following expression for the equilibrium vacancy concentration:[35]

$$C_v^{eq} = 23 \exp\left(-\frac{0.66 \text{ eV}}{kT}\right) \quad [24]$$

The strain-induced vacancies are considered at 2.7 pct strain and 0.55 s^{-1} strain rate, as used in the experiment. Experimental results are also shown along with the predictions based on the mechanical jog model. Thus, at a strain-rate of 0.55 s^{-1}, thermal vacancies dominate at temperatures above about 550 K while the strain-induced vacancies become dominant at lower temperatures. The deformation-induced vacancy concentration increases exponentially as lower temperatures are approached, attaining a relatively temperature-independent value at temperatures below about 300 K, this is the transition temperature, T^*, noted earlier. In this low-temperature region, the deformation-induced vacancy concentration is controlled by plastic strain.

VI. SUMMARY

The NMR relaxation rates determined in Al during deformation using the CUT-sequence pulse technique enabled a direct evaluation of the strain-induced vacancy concentration. The temperature, strain, and strain-rate effects on NSR rates clearly delineated the temperature regimes, where strain-induced vacancy concentration dominates the thermal equilibrium vacancy concentration. Two distinct temperature regimes are found, where strain-induced vacancies become dominant. At low temperatures, the excess vacancies are temperature independent and increase linearly with plastic strain. At high temperatures above a critical value, the strain-induced vacancy concentration decreases with increasing temperature due to *in situ* annealing. The present study clearly reveals the power and applicability of NMR pulse techniques in characterizing *in situ* the dynamical behavior of point defects in a noninvasive fashion.

ACKNOWLEDGMENTS

The work was supported by the Deutsche Forschungsgemeinschaft and the Foundation for Fundamental Research on Matter (FOM). We acknowledge the travel grants provided by the Government of Nordrhein-Westfalen and the North Carolina Board of Science and Technology.

This article is based on a paper presented at *Nondestructive Evaluation (NDE) and Materials Properties III*, TMS Fall Meeting, Cincinnati, OH, Oct. 1996.

REFERENCES

1. K. Linga Murty, K. Detemple, O. Kanert, G. Peters, and J.Th. DeHosson: *J. Mater. Sci.*, 1996, vol. 31, p. 3289.
2. K.L. Murty, F.A. Mohamed, and J.E. Dorn: *Scripta Metall.*, 1971, vol. 5, p. 1087; P.G. McCormick and K.L. Murty: *Scripta Metall.*, 1972, vol. 6, p. 225.
3. H. Mecking and Y. Estrin: *Scripta Metall.*, 1980, vol. 14, p. 815.
4. A.L. Ruoff: *J. Appl. Phys.*, 1967, vol. 38, p. 3999; A.L. Ruoff: in *Lattice Defects and Their Interactions*, R.R. Hasiguti, ed., Gordon and Breach, New York, NY, 1966, p. 961.
5. T. Watanabe and S. Karashima: *Phys. Status Solidi*, 1970, vol. 42, p. 747.
6. K. Linga Murty: *Mater. Sci. Eng.*, 1974, vol. 14, p. 217.
7. K. Linga Murty, M. Gold, and A.L. Ruoff: *J. Appl. Phys.*, 1970, vol. 41, p. 4917.
8. H. Murakami and S. Yoshida: *Cryst. Lattice Defects*, 1975, vol. 6, p. 89.
9. A. Jackman, G.M. Hood, and R.J. Schult: *J. Phys.*, 1987, vol. F17, p. 1817.
10. B. Wodniecka, M. Marszalek, and P. Wodniecki: *J. Phys. Cond. Mat.*, 1989, vol. 1, p. 7512.
11. K. Sassa, W. Petry, and G. Vogl: *Phil. Mag.*, 1983, vol. 48, p. 1.
12. G. Guenin, J. Perez, and P.F. Gobin: *Cryst. Lattice Defects*, 1972, vol. 3, p. 199.
13. O. Kanert: *Phys. Rep.*, 1982, vol. 91, p. 183.
14. N. Bloembergen, E.M. Purcell, and R.V. Pound: *Phys. Rev.*, 1948, vol. 73, p. 679.
15. C.P. Slichter: *Principles of Magnetic Resonance*, Springer, Berlin, 1990.
16. K.L. Murty and A.L. Ruoff: *Phys. Rev.*, 1970, vol. B1, p. 114.
17. T.J. Rowland and F.Y. Fradin: *Phys. Rev.*, 1969, vol. 182, p. 760.
18. H.J. Hackeloer, O. Kanert, H. Tamler, and J.Th. DeHosson: *Rev. Sci. Instrum.*, 1983, vol. 54, p. 341.
19. W.H.M. Alsem, J.Th. DeHosson, H. Tamler, and O. Kanert: *Phil. Mag.*, 1982, vol. 46, p. 451.
20. K.L. Murty and O. Kanert: *J. Appl. Phys.*, 1990, vol. 67, p. 2866.
21. K. Detemple, O. Kanert, K.L. Murty, and J.Th. DeHosson: *Phys. Rev.*, 1995, vol. B52 (1), p. 125.
22. C.P. Ling and P.G. McCormick: *Acta Metall.*, 1993, vol. 41, p. 3127.
23. A.L. Ruoff and R.W. Balluffi: *J. Appl. Phys.*, 1963, vol. 34, p. 1848; 1963, vol. 34, p. 2862.
24. K. Detemple, O. Kanert, K.L. Murty, and J.Th. DeHosson: *Phys. Rev.*, 1991, vol. B44 (5), p. 1988.
25. K. Hirano, M. Cohen, B.L. Averbach, and N. Ujiye: *Trans. AIME*, 1963, vol. 227, p. 950.
26. A.R. Wazzan and J.E. Dorn: *J. Appl. Phys.*, 1965, vol. 36, p. 222.
27. C.H. Lee and R. Maddin: *Trans. AIME*, 1959, vol. 215, p. 397.
28. C.G. Lenasson: *Scripta Metall.*, 1972, vol. 14, p. 1125.
29. U.F. Kocks: *J. Eng. Mater. Technol.*, 1976, vol. 14, p. 76.
30. E.D. Ostroff and J.S. Waugh: *Phys. Rev. Lett.*, 1966, vol. 16, p. 1096.
31. W.K. Rhim, D.P. Burum, and D.D. Ellemann: *J. Chem. Phys.*, 1978, vol. 68, p. 692.
32. W. Grunder, H. Schmiedel, and D. Freude: *Ann. Phys.*, 1971, vol. 27, p. 409.
33. F.Y. Fradin and T.J. Rowland: *Appl. Phys. Lett.*, 1967, vol. 11, p. 207.
34. J.E. Bird, A.K. Mukherjee, and J.E. Dorn: in *Quantitative Relations between Properties and Microstructure*, D.G. Brandon and A. Rosen, eds., Israel University Press, Jerusalem, 1969.
35. A. Seeger, D. Wolf, and H. Mehrer: *Phys. Status Solidi*, 1971, vol. B48, p. 481.